Optics Letters

# Localized plasmonic structured illumination microscopy with gaps in spatial frequencies

Anna Bezryadina,[1,†] Junxiang Zhao,[1,†] Yang Xia,[2] Yeon Ui Lee,[1] Xiang Zhang,[2] and Zhaowei Liu[1,*]

[1]Department of Electrical and Computer Engineering, University of California, San Diego, La Jolla, California 92093, USA
[2]Department of Mechanical Engineering, University of California, Berkeley, California 94720, USA
*Corresponding author: zhaowei@ucsd.edu

Received 6 March 2019; revised 22 April 2019; accepted 8 May 2019; posted 13 May 2019 (Doc. ID 361780); published 31 May 2019

**Localized plasmonic structured illumination microscopy (LPSIM) is a super-resolution fluorescent microscopy method to image samples at a high speed with a wide field of view and low phototoxicity. Here we propose a methodology to extend the resolution capability of LPSIM by shifting spatial frequencies farther away from the diffraction-limited cutoff frequency with a plasmonic nano-array. We analyze the performance and accuracy of image reconstruction by using simulations of standard structured illumination microscopy (SIM) and blind-LPSIM. LPSIM experiments were also performed by using various LPSIM substrates and different microscope objectives. The experiments and simulations show that by shifting spatial frequencies farther away, resolution improvement can be extended up to 5 times beyond the diffraction limit with minimal deformation and artifacts in the reconstructed image.** 

https://doi.org/10.1364/OL.44.002915

Super-resolution light microscopy techniques have extended the understanding of sub-cellular biological structure and dynamics to nanoscale using fluorescent microscopy. In the past decade, numerous super-resolution microscopy methods, including stochastic optical reconstruction microscopy [1–3], photo-activated localization microscopy [4,5], stimulated emission depletion microscopy [6,7], and structured illumination microscopy (SIM) [8–23] are developed to extend the resolution capability beyond the diffraction limit.

Localized plasmonic structured illumination microscopy (LPSIM) [24–28] utilizes the near-field resonance of a periodical nano-antenna array to bring the high spatial frequency information of the object into the detectable bandwidth of a microscope. LPSIM has experimentally demonstrated three-fold resolution improvement, compared to diffraction-limited microscopy, and achieved 50 nm full width at half-maximum (FWHM) resolution and video speed for dynamic biological samples [28].

For best performance, the LPSIM substrates that contain the hexagonal patterned periodical silver nanodiscs, are designed to match the high numerical aperture (NA) water-immersion or oil-immersion objective lens [24,26]. However, such objectives, in general, are expensive and are not easily switchable during a biological experiment. In certain applications, a low NA air objective is preferred to provide a larger field of view at the cost of lower resolution.

In this Letter, we studied the performance of LPSIM when the illumination patterns contain spatial frequencies much higher than the cutoff frequency of the optical transfer function (OTF). The amount of detection area and missing information in the spatial frequency domain can be controlled by changing the NA of the objective and emission wavelength of fluorophores, which affect the size of the OTF, or by changing the dimensions of the LPSIM pattern, which affect the shift amount of the OTF in k-space due to frequency mixing of object information [Figs. 1(a)–1(c)]. In our experiments, we used an LPSIM substrate with 145 and 135 nm pitch distance and a 60 nm silver disc diameter, in combination with low and high NA objectives. In our simulations, we varied the NA of objectives and dimensions of periodic patterns (200, 150, and 100 nm pitch distance and 80 and 60 nm disc diameter). We investigated the resolution capability of LPSIM, combined with a blind-SIM reconstruction algorithm [29,30] when the spatial frequency shift due to the patterned nano-antenna array is two times greater than the diffraction-limited cutoff frequency. Our results showed that, although a significant portion of k-space information is missing, the accuracy of reconstructed images by using LPSIM with blind-SIM algorithm is significantly higher compared to standard SIM image reconstruction. To improve the resolution capability and the robustness of the reconstruction process, we used more sub-images than standard SIM or the original LPSIM system to oversample the object information in collected sub-images.

In our experimental setup, we modified ab Olympus IX83 inverted microscope to achieve the reflection mode for LPSIM imaging [Fig. 1(d)] [26,28]. For multiple-angle illumination of fluorescent sample on top of the LPSIM substrate, the collimated 1–2 $mm^2$ excitation beam from a Genesis MX488 laser (Coherent) was steered by a pair of galvo mirrors and then projected by using a 4f system to the focal plane of the LPSIM substrate. To guarantee the TM polarization for illuminating the LPSIM substrate, the beam was sent through a custom-made polarizer plate, which consists of 12 polarizing stripes.

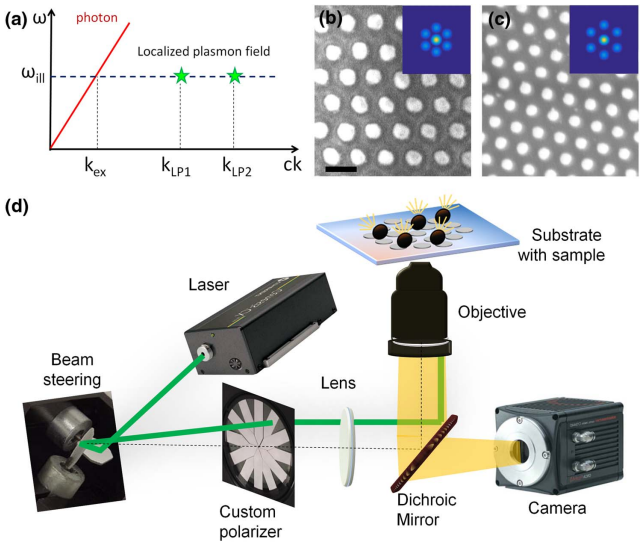


**Fig. 1.** Concept and experimental set-up. (a) Illustrative plot of temporal frequency *versus* wavenumber for the illuminating laser. By tuning the dimensions of the fabricated nano-antenna array, different spatial frequencies $k_{LP}$ can be generated. (b), (c) Top-view SEM images of a nanodisc array, showing silver discs arranged in a hexagonal lattice with a disc diameter of 80 and 60 nm and pitch of 200 and 145 nm, respectively. Inserts: corresponding effective total OTF of the LPSIM system with a 0.8 NA objective. Only the 0 order and first order are considered. The scale bars represent 200 nm. (d) Schematics of the LPSIM experimental imaging setup.

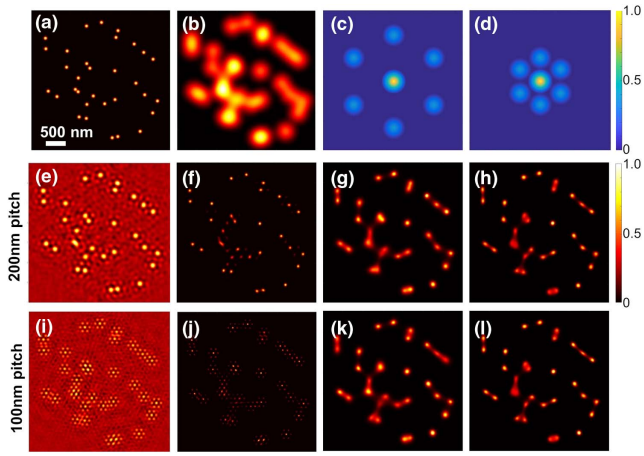


**Fig. 2.** Comparison of simulated imaging results for different reconstruction methods by using a 0.80 NA objective with 200 and 100 nm periodicity cosine illumination patterns. (a) Ground truth image of a distribution of 10 nm circular objects. (b) Diffraction-limited image. (c), (d) Effective total OTF for 100 and 200 nm illumination periodicity, respectively. (e), (i) Regular SIM super-resolution image before deconvolution. Significantly more reconstruction artifacts observed in the image with 100 nm illumination patterns due to large missing information in Fourier space. (f), (j) Lucy deconvolution of regular SIM using the corresponding OTF. (g), (k) Blind-LPSIM with nine sub-images. (h), (l) Blind-LPSIM with 30 sub-images.

The fluorescent signal from the sample was collected by an objective in the reflection mode and imaged with a sCMOS camera (ORCA_Flash4.0 V3, Hamamatsu). A National instruments DAQ module (NI-9263) controlled by MATLAB is used to change the incident angles of the laser beam onto an LPISM substrate with up to 800 Hz, as well as to synchronize the camera to take and save all images. The laser power density is typically less than 20 $W/cm^2$.

To demonstrate the effect of missing k-space information on reconstructed super-resolution images, we tested the performance of both standard SIM combined with deconvolution and LPSIM with a blind-SIM algorithm using dot objects illuminated by periodical patterns with different spatial frequencies (Fig. 2). In the simulation, we used circular objects of 10 nm in diameter and a periodical sinusoidal illumination pattern with 100 and 200 nm periodicity. The simulation was performed with a 0.8 NA objective and 570 nm emission wavelength. For standard SIM reconstruction, we solve the linear system of the three information components for each illumination pattern orientation in Fourier space [8,15]. The recovered Fourier space components of the object are then shifted to their corresponding true locations. Shown in Figs. 2(c) and 2(d) are the effective total OTFs corresponding to 100 and 200 nm illumination periodicity. Figures 2(e), 2(f), 2(i), and 2(j) show the reconstructed images of standard SIM with and without Lucy deconvolution. When too much information from the object is missing in the Fourier domain, the reconstructed images contain significant amount of artifact using standard SIM reconstruction. With 100 nm illumination periodicity, the gaps in k-space caused significant side lobes for each dot object in the reconstructed image [Fig. 2(j)]. In comparison, the reconstruction artifact is significantly reduced when using an LPSIM illumination pattern with blind-SIM image reconstruction. Blind-SIM reconstruction finds an optimized object as a constrained joint-deconvolution in real space for all acquired sub-images with different areas being illuminated, thus generating super-resolution images with reduced artifacts. Shown in Figs. 2(g), 2(k), 2(h), and 2(l) are blind-SIM reconstructed images with nine sub-images and 30 sub-images. The oversampled data sets were generated by increasing the scanning angle in each $x$–$y$ direction determined by the LPSIM substrate and the corresponding polarization plate.

A standard 2D SIM image reconstruction requires only nine sub-images with three sub-images on each of the three different illumination directions. However, since blind-SIM algorithm reconstructs the super-resolution image in real space using a cost-minimization approach, by having more illumination directions for LPSIM, we create illumination patterns with better uniformity as the localized plasmon mode changes with illumination angles. 30 sub-images are collected from six illumination directions with five sub-images per each direction. The LPSIM reconstructed images with 30 sub-images provide higher resolution compared to LPSIM images with nine sub-images while having a minimum amount of artifacts, even with a large amount of missing information in k-space. The FWHM decreases ~4.5 times from 367 nm for a diffraction-limited image down to 82 nm for blind-SIM algorithm with 30 LPSIM sub-images.

Since in the experiment the pitch distance of LPSIM substrates cannot be changed, the gap in Fourier space was adjusted by changing objective lens. To test the super-resolution capability of LPSIM with missing Fourier space information,

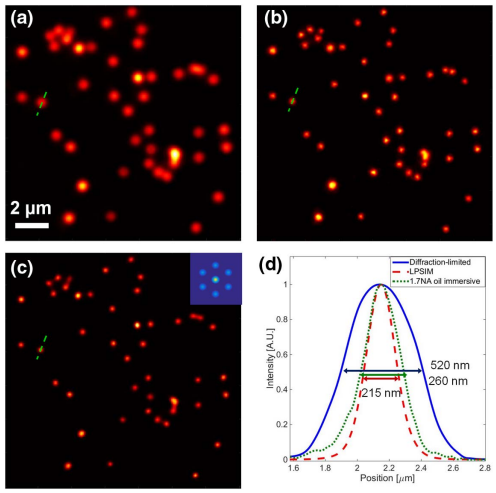


**Fig. 3.** Experimental results for 200 nm orange beads on top of LPSIM substrate with 145 nm pitch. (a) Diffraction-limited images under a 0.60 NA objective. (b) Diffraction-limited images under a 1.70 NA objective. (c) Blind-LPSIM reconstruction image. Inserts: OTF for a 0.60 NA objective and 145 nm illumination periodicity pattern. (d) Normalized intensity profile of the images in (a)–(c) along the dashed green lines. The FWHM of the orange bead goes down to 215 nm.

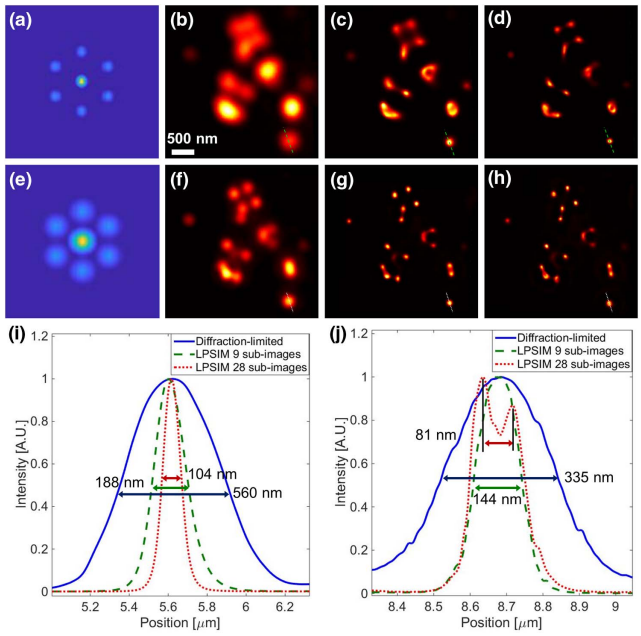


**Fig. 4.** Experimental results for blind-LPSIM with 45 nm orange beads under a 0.55 NA objective (top row) and a 1.20 NA objective (bottom row) on top of an LPSIM substrate with 135 nm in pitch. (a), (e) OTF for a 0.55 NA objective and a 1.20 NA objective, respectively. (b), (f) Diffraction-limited images. (c), (g) Blind-LPSIM reconstruction images with nine sub-images. (d), (h) Blind-LPSIM reconstruction images with 27 sub-images. (i) Normalized intensity profile of the images in (b)–(d) along the dashed green lines. The FWHM of the orange bead is resolved down to 104 nm. (j) Normalized intensity profile of the images in (f)–(h) along the dashed white lines. Two beads were resolved with 27 sub-images.

200 nm orange fluorescent polystyrene beads (540/560 nm) were drop-casted on to an LPSIM substrate of 60 nm diameter silver discs and 145 nm pitch distance and were imaged through a 0.6 NA objective [Fig. 3(a)]. Figure 3(b) shows the image of the same area using a 1.7 NA oil-immersion objective for providing a high-resolution comparison. In the blind-LPSIM reconstructed image with nine sub-images [Fig. 3(c)] the FWHM resolution of a single 200 nm bead was improved from 520 nm down to 215 nm [Fig. 3(d)], and closely spaced beads were clearly resolved. As shown in the inset of Fig. 3(c), significant part of collected k-space information was missing; however, the blind-SIM managed to reconstruct a high-resolution image without introducing visible artifacts.

To demonstrate the effect of oversampling in LPSIM and ability to resolve fine sample features, 45 nm orange fluorescent beads (540/560 nm) were drop-casted on an LPSIM substrate with a 60 nm silver disc in diameter and 135 nm in pitch, and imaged through 0.55 NA and 1.2 NA objectives. The data set with a 0.55 NA objective had large gaps in Fourier space with a lot of relevant information missing [Fig. 4(b)], and the data set with a 1.20 NA objective had small gaps in Fourier space [Fig. 4(f)]. For both sets of data, the reconstruction of LPSIM super-resolution images was done with nine sub-images (three angles of illumination) and 27 sub-images (six angles of illumination), as shown in Figs. 4(c), 4(d), 4(g), and 4(h). Using oversampled data sets of a 0.55 NA objective, the FWHM resolution of the beads improved from 188 nm for reconstruction using nine sub-images to 104 nm for reconstruction using 27 sub-images, where the diffraction-limited image had a FWHM of 560 nm [Fig. 4(i)]. With the data set of a 1.20 NA objective, which had less gap in collected k-space information, a single dot is resolved as two closely spaced dots with peak-to-peak distance of 81 nm in blind-LPSIM reconstruction using 27 sub-images, which is otherwise un-resolved when using only nine sub-images [Figs. 4(h) and 4(j)]. Oversampling helped to resolve finer details and achieve more than 5 times resolution improvement for a 0.55 NA objective and more than 4 times resolution improvement for a 1.20 NA objective. Unfortunately, when a large part of k-space information is missing, oversampling cannot completely compensate for the missed information in the gaps between spatial frequencies peaks and creates additional artifacts in the reconstructed image.

To demonstrate the advantage of LPSIM with blind reconstruction and show how reconstruction algorithms work for non-sparse object, we simulate standard SIM and blind-SIM with LPSIM illumination using a solid striped object (Fig. 5). The images are generated using 1.2 NA and 0.55 NA objectives, and the periodicity of the illumination pattern is 150 nm. Figures 5(c)–5(f) show the reconstructed striped object with standard SIM, SIM with Weiner deconvolution, SIM with Lucy deconvolution, and blind-LPSIM for a 1.2 NA objective. Without too much missing information, both SIM and LPSIM reconstruct accurate super-resolution images compared to ground truth shown in Fig. 5(a). When using the same periodicity in illumination and a smaller NA objective, the effect of missing information in Fourier domain becomes much more significant, as shown in Figs. 5(i)–5(k), where the reconstructed images of SIM, SIM with Weiner deconvolution, and SIM with Lucy deconvolution is plotted. In contrast, the

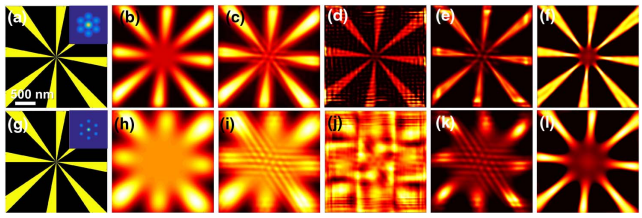


**Fig. 5.** Comparison of reconstruction methods for a non-sparse complex image under a 1.20 NA objective (top row) and a 0.55 NA objective (bottom row) with a 150 nm illumination periodicity pattern (a), (g) Initial image of a star-shaped object. Inserts: effective total OTF for a 1.20 NA objective and a 0.55 NA objective, respectively. (b), (h) Diffract ion-limited images. (c), (i) Regular SIM. (d), (j) Wiener deconvolution of regular SIM. (e), (k) Lucy deconvolution of regular SIM. (f), (l) Blind-LPSIM reconstruction.

blind-LPSIM image shown in Fig. 5(j) contains fewer artifacts at a cost of slightly lower resolution. The blind-LPSIM method is more robust in resolving images with large gaps in k-space information. The experimental ability of SIM and LPSIM to resolve non-sparse complex objects were demonstrated before by video imaging of microtubules dynamics at several hertz speed [9,28].

In conclusion, we showed how a standard SIM and blind-SIM with LPSIM substrate methods worked when a part of spatial frequency is missing in reconstruction. The blind-SIM method with LPSIM shows robust reconstruction with much fewer artifacts. In addition, by decreasing the pitch size of LPSIM substrates, the reconstruction resolution of the image can be improved from 3 times to 4–5 times in comparison to a diffraction-limited image. Furthermore, by developing new LPSIM substrates with 80 nm pitch size and implementing a 1.70 NA objective, we can push resolution down to 30–40 nm while preserving a large field of view, biocompatibility, and several hertz speed.

**Funding.** National Science Foundation (NSF) (CBET-1604216); Gordon and Betty Moore Foundation.

**Acknowledgment.** The authors thank Eric Huang for his useful comments.

†These authors contributed equally to this Letter.

## REFERENCES

1. B. Huang, W. Q. Wang, Bates, and X. W. Zhuang, Science **319**, 810 (2008).
2. M. J. Rust, M. Bates, and X. Zhuang, Nat. Methods **3**, 793 (2006).
3. K. Xu, H. P. Babcock, and X. Zhuang, Nat. Methods **9**, 185 (2012).
4. E. Betzig, G. H. Patterson, R. Sougrat, O. W. Lindwasser, S. Olenych, J. S. Bonifacino, M. W. Davidson, J. Lippincott-Schwartz, and H. F. Hess, Science **313**, 1642 (2006).
5. S. Manley, J. M. Gillette, G. H. Patterson, H. Shroff, H. F. Hess, E. Betzig, and J. Lippincott-Schwartz, Nat. Methods **5**, 155 (2008).
6. K. I. Willig, B. Harke, R. Medda, and S. W. Hell, Nat. Methods **4**, 915 (2007).
7. S. W. Hell and J. Wichmann, Opt. Lett. **19**, 780 (1994).
8. M. G. L. Gustafsson, J. Microsc. **198**, 82 (2000).
9. P. Kner, B. B. Chhun, E. R. Griffins, L. Winoto, and M. G. L. Gustafsson, Nat. Methods **6**, 339 (2009).
10. L. Schermelleh, P. M. Carlton, S. Haase, L. Shao, L. Winoto, P. Kner, B. Burke, M. C. Cardoso, D. A. Agard, M. G. Gustafsson, H. Leonhardt, and J. W. Sedat, Science **320**, 1332 (2008).
11. Y. Blau, D. Shterman, G. Bartal, and B. Gjonaj, Opt. Lett. **41**, 3455 (2016).
12. M. G. L. Gustafsson, Proc. Natl. Acad. Sci. USA **102**, 13081 (2005).
13. D. Li, L. Shao, B. Chen, X. Zhang, M. Zhang, B. Moses, D. E. Milkie, J. R. Beach, J. A. Hammer III, M. Pasham, T. Kirchhausen, M. A. Baird, M. W. Davidson, P. Xu, and E. Betzig, Science **349**, aab3500 (2015).
14. F. Ströhl and C. F. Kaminski, Optica **3**, 667 (2016).
15. A. Lal, C. Shan, and P. Xi, IEEE J. Sel. Top. Quantum Electron. **22**, 6803414 (2016).
16. E. H. Rego, L. Shao, J. J. Macklin, L. Winoto, G. A. Johansson, N. Kamps-Hughes, M. W. Davidson, and M. G. L. Gustafsson, Proc. Natl. Acad. Sci. USA **109**, E135 (2012).
17. R. Heintzmann, T. M. Jovin, and C. Cremer, J. Opt. Soc. Am. A **19**, 1599 (2002).
18. R. Heintzmann and M. Gustafsson, Nat. Photonics **3**, 362 (2009).
19. R. Diekmann, Ø. I. Helle, C. I. Øie, P. McCourt, T. R. Huser, M. Schüttpelz, and B. S. Ahluwalia, Nat. Photonics **11**, 322 (2017).
20. F. Wei, D. Lu, H. Shen, W. Wan, J. L. Ponsetto, E. Huang, and Z. Liu, Nano Lett. **14**, 4634 (2014).
21. A. G. York, S. H. Parekh, D. Dalle Nogare, R. S. Fischer, K. Temprine, M. Mione, A. B. Chitnis, C. A. Combs, and H. Shroff, Nat. Methods **9**, 749 (2012).
22. Q. Wang, J. Bu, P. S. Tan, G. H. Yuan, J. H. Teng, H. Wang, and X. C. Yuan, Plasmonics **7**, 427 (2012).
23. A. I. Fernández-Domínguez, Z. Liu, and J. B. Pendry, ACS Photonics **2**, 341 (2015).
24. J. L. Ponsetto, F. Wei, and Z. Liu, Nanoscale **6**, 5807 (2014).
25. S. Liu, C.-J. Chuang, C. W. See, G. Zoriniants, W. L. Barnes, and M. G. Somekh, Opt. Lett. **34**, 1255 (2009).
26. J. L. Ponsetto, A. Bezryadina, F. Wei, K. Onishi, H. Shen, E. Huang, L. Ferrari, Q. Ma, Y. Zou, and Z. Liu, ACS Nano **11**, 5344 (2017).
27. A. Bezryadina, J. Li, J. Zhao, A. Kothambawala, J. Ponsetto, E. Huang, J. Wang, and Z. Liu, Nanoscale **9**, 14907 (2017).
28. A. Bezryadina, J. Zhao, Y. Xia, X. Zhang, and Z. Liu, ACS Nano **12**, 8248 (2018).
29. E. Mudry, K. Belkebir, J. Girard, J. Savatier, E. Le Moal, C. Nicoletti, M. Allain, and A. Sentenac, Nat. Photonics **6**, 312 (2012).
30. R. Ayuk, H. Giovannini, A. Jost, E. Mudry, J. Girard, T. Mangeat, N. Sandeau, R. Heintzmann, K. Wicker, K. Belkebir, and A. Sentenac, Opt. Lett. **38**, 4723 (2013).